M-Estimator Application in Real-Time Sensor Fusion for Smooth Position Feedback of Heavy-Duty Field Robots

Henri Liikanen
Unit of Automation Technology and Mechanical Engineering
Tampere University
Tampere, Finland
henri.liikanen@tuni.fi

Mohammad M. Aref
Unit of Automation Technology and Mechanical Engineering
Tampere University
Tampere, Finland
m.aref@ieee.org

Jouni Mattila
Unit of Automation Technology and Mechanical Engineering
Tampere University
Tampere, Finland
jouni.mattila@tuni.fi

***Abstract*—In this paper, we study the performance of a complementary filter with adaptive weights in sensor fusion application for real-time localization of an omnidirectional field robot. The test-case robot is a large, four-wheel drive and steer (4WDS), construction vehicle with nonlinear internal dynamics and hydraulic driving and steering actuators. Our objective is to provide the real-time controller of the vehicle with a robust and smooth feedback that prevents unnecessary oscillations of steering, which can waste significant amount of energy. This is done by assigning weights for measurements based on their consistency with the robot's motions. The calculations are based on two main data sources: (1) measured velocities vectors from wheel driving (odometer) and steering of the 4WDS test-case robot as well as (2) data obtained from a differential Global Navigation Satellite System (GNSS) for absolute pose of the robot. We show that the fusion is robust to the noise and single point failures of the sensors while the maximum heading oscillations are reduced by 70−95% that preserves accuracy of the global positioning system. Moreover, we demonstrated feasibility and efficacy of the real-time implementation of this filtering method on the path-following control of the robot.**

Keywords—sensor fusion, motion estimation, path following, heavy-duty field robot, GNSS, GPS, wheel odometry

I. INTRODUCTION

Interests towards the study field of autonomous vehicles (AV) have grown considerably during the last decade. For autonomous driving on predefined paths, state-of-the-art path-following controllers are able to control robots with accuracies measured in centimeters [1], [2]. However, in order to achieve these accuracies, controllers require the received positioning feedback to be precise, robust, and smooth but not delayed. Absolute positioning of a field robot is most of the times implemented using GNSS. To the best of the authors' knowledge, even the high-cost GNSS-systems all alone are not able to produce positioning that is smooth and robust enough for accurate path-following control, without oscillations in the steering. With heavy-duty field robots, these oscillations will produce massive unnecessary forces between the tire and terrain, which waste energy and will eventually lead to premature wearing of the tires and moving structures.

Comprehensive studies have been conducted on sensor fusion for vehicle positioning. In one of the latest ones [3], single automotive radar and a gyroscope was used to provide complete odometry estimation for the position. The study showed good results, especially for replacing wheel- or visual-odometry with the suggested method during slippery ground and low visibility circumstances. However, including the absolute position was not considered; the GNSS was used as a ground truth reference. For fusion of GPS and odometry, the authors in [4] fuse a relative odometry with included gyroscope with an absolute GPS position to estimate robot localization. They proved that the fusion of odometry and gyroscope with Kalman filtering provided accurate indoor measurements, where the traveled distances were under 100 m. However, the GNSS technology of the time had a constant localization error of 0.8 m, which is why the outdoor results obtained at the time cannot be compared to results gathered with the current existing GNSS technology. In [5], the authors used the extended Kalman filter to fuse differential-GPS and odometry to localize a mobile robot. Feasibility of the fused signal was evaluated in a mobile robot teleoperation experiment, where the fusion result showed that the deviation from the GPS-based ground truth was under of 20 cm even during the turning situation. In addition to the studies introduced, authors of this paper did not find any studies from the past 5 years, where the pure wheel odometry and GNSS had been used for smooth motion estimation of field robots.

This paper focus on fusing a noisy, variable-delayed, but absolute GNSS position to a smooth and low latency wheel odometry feedback to form an accurate and robust feedback signal, which can be given in real-time to a control system as a localization feedback. The fusion is based on M-estimator application introduced in [6], where originally the absolute position was received based on vision. In this paper, we are using the GNSS to prove the high performance of the selected algorithm for alternative sensors. Furthermore, we are applying the fusion into a heavy-duty omnidirectional construction vehicle with nonlinear internal dynamics and high inertia. The experimental test-case robot, four-wheel drive and steer (4WDS) Haulotte, is shown in Fig. 1.

This paper is organized as follows: in section II, the architecture and sensor configurations of the test-case robot are presented. Software and algorithms are introduced in section III. Results from the fusion and path-following control with the fused feedback are shown in section IV. Finally, we conclude the study in V and suggest the main key features to be focused on in the future research.

Fig. 1. Heavy-duty test-case robot Haulotte 16 RTJ PRO in the experimental environment.

II. Robot Architecture

A. Test-Case Robot: Haulotte 16 RTJ PRO

Haulotte is a heavy-duty, four-wheel drive and steer (4WDS), articulated boom lift with hydraulic driving and steering actuators [7]. Usually these types of vehicles are used as mobile bases for aerial work platforms. The robot weights 6650 kg and its boom can lift objects up to 15 m. The dimensions and parameters of the robot, relevant to the study, are presented in Table I and Fig. 2.

A diesel engine, powers a variable-displacement hydraulic pump, which provides the oil flows to all the actuators. Robot's wheels are driven by four fixed-displacement hydraulic motors. The motors' revolution speeds are separately controlled with four hydraulic servo valves. The valve openings are controlled using velocity-based PI-controllers with included feedforward terms. The wheels are steered using two symmetrical hydraulic cylinders, actuated by two proportional valves. These valves are proportionally controlled. [7]

B. Sensor Configurations

For autonomous driving, the robot has a Beckhoff CX2030 real-time hardware platform, which has a wide modularity for interfacing with various sensors and actuators. The platform runs TwinCAT software system. The programming is executed in MATLAB Simulink environment and the developed modules are built for the target of TwinCAT system. The robot has a wireless communication between the real-time hardware and the host PC.

Each wheel of the test-case robot has a metallic rotating disk with 150 equally distributed holes and two optical sensors

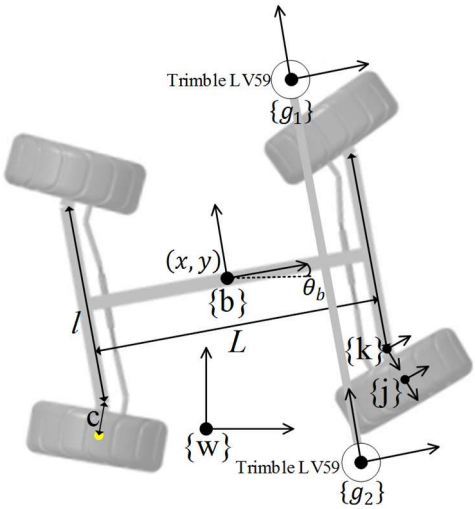

Fig. 2. Denoted coordinate frame and main dimensions of the test-case robot.

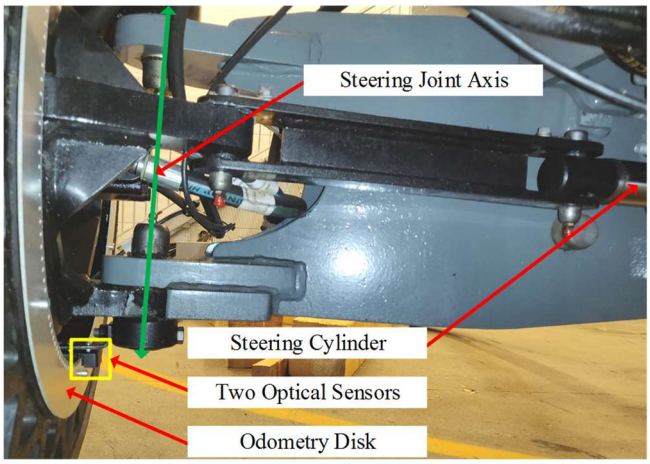

Fig. 3. The optical sensors and metallic disk used for measuring wheel odometry. See the marked steering cylinder and joint of the frame {k} presented in Fig. 2.

for sensing the holes, see Fig. 3. The velocity of the wheel is derived from the sensed pulses. These types of robots are usually driven quite slow, by using speeds less than 5 km/h. For this reason, optical sensors were used instead of hall-effect sensors to improve pulses per round ratio and obtain a high resolution output. As it is presented in [8], while using hall-effect sensors, the resolution of the encoder becomes large and during a low speed motion, limited amount of pulses are generated. This type of behavior causes problems for controller feedback.

Low-cost incremental wire encoders are used for measuring the displacements of the steering cylinders. With the known dimensions of the steering structures, the measured cylinder displacement is mapped as a steering angle of the frame {k} with respect to the base frame {b}, see Fig. 2.

For absolute outdoor positioning, the robot has a Novatron BX982 differential carrier-phase GNSS receiver benefited from online correction factors and with two Trimble LV59 antennas, see Fig. 1. The locations of the antennas and their respective coordinate frames are illustrated in Fig. 2. The distance between the antennas is 2.6 m. The left antenna $\{g_1\}$ is used for receiving the position and right $\{g_2\}$ to from the heading vector together with the left one. The GPS heading angle, mapped to the base frame {b} of the robot is to be further on marked as θ_g. The GPS is using Real-time kinematic (RTK) correction reference, which is received from a commercial base station located 13 km from the experiment area. With the correction, accuracies for positioning and heading vector are ± 0.03 cm and 0.09 deg. Data rate of the GNSS is 50 Hz. The communication between the GNSS receiver and real-time hardware platform is conducted via Ethernet user datagram protocol (UDP).

TABLE I
General specifications of the test-case robot.

Description	Quantity
Distance between front and rear wheel axle (L)	2.1 m
Distance between wheel axle's steering joints (l)	1.46 m
Distance between steering joint and wheel center (c)	0.24 m
Wheel diameter	0.854 m
Mass of the robot	6650 kg
Approximate maximum linear wheel velocity (4WS)	0.36 m/s

III. Software and Algorithms

A. Software

Modular structure of the software running in the Beckhoff real-time hardware PC is illustrated in Fig. 4. The entire closed-loop control system together with the robot is thoroughly discussed in [7]. In this paper, the focus is in the highlighted modules and in the final output that is sent by them to the Controller module.

Motion Estimation module includes the algorithms presented in the following subsection C. The nominal placement of the switch after Forward Kinematics illustrates that with the experimental cases 1 and 2 in section IV, the control loop was closed with pure wheel odometry feedback and the data was synchronously gathered in the Data Logging block. Results from closing the control loop through the Motion Estimation in real-time are shown in cases 3 and 4.

B. Forward Kinematics

Measured wheel velocities and steering angles of each wheel are mapped to a specific base frame {b} of the target robot. The mapping is based on the least-square solution presented in [9]. Linear- and angular-velocity components of the base frame {b} in planar motion are presented as follows

$$\begin{bmatrix} v_{bx}^{w} \\ v_{by}^{w} \\ \dot{\theta}_{bz}^{w} \end{bmatrix} = \boldsymbol{A}^{\dagger}\boldsymbol{B}, \text{ where } \boldsymbol{A}^{\dagger} = (\boldsymbol{A}\boldsymbol{A}^{T})^{-1}\boldsymbol{A}^{T}, \tag{1-2}$$

$$\boldsymbol{A}^{T} = \begin{bmatrix} 1 & 0 & \dots & 1 & 0 \\ 0 & 1 & \dots & 0 & 1 \\ -r_{1y} & r_{1x} & \dots & -r_{4y} & r_{4x} \end{bmatrix}_{3x8}, \tag{3}$$

$$\boldsymbol{B}^{T} = [v_{1x} \quad v_{1y} \quad \dots \quad v_{4x} \quad v_{4y}]_{1x8}. \tag{4}$$

Elements of **B** represent the measured velocity components of the wheel frames. The elements of **A** represent vectors measured from the base frame {b} to the wheel frames {j}. Unlike in [9], in our solution the elements vary as functions of the measured steering angles and structural dimensions, see Fig. 2. Therefore, the pseudoinverse of **A** is calculated in each control cycle. Results shown in Fig. 7 of section IV from back propagating the base frame velocity components to linear wheel velocities and comparing them to their corresponding measured feedbacks proves our solution for the kinematic mapping to be accurate and robust.

C. Motion Estimator

Fusion between position-based GPS and incremental velocity-based odometry is conducted by adaptation of the complementary filtering approach presented in the application [6] for integration of visual feedback in a control loop. In our solution, the incrementally measured θ_{bz} and GPS-based θ_g heading angles are fused by considering the differential (5)

$$\begin{bmatrix} \dot{\hat{Z}}_{\theta} \\ \dot{\hat{b}}_{\theta} \end{bmatrix} = \boldsymbol{C}\begin{bmatrix} \hat{Z}_{\theta} \\ \hat{b}_{\theta} \end{bmatrix} + \omega_{\theta}\begin{bmatrix} k_{P,\theta} \\ k_{I,\theta} \end{bmatrix}(\theta_g - \hat{Z}_{\theta}) + \boldsymbol{D}\dot{\theta}_{bz}, \tag{5}$$

where,

$$\boldsymbol{C} = \begin{bmatrix} 0 & 1 \\ 0 & 0 \end{bmatrix} \text{ and } \boldsymbol{D} = \begin{bmatrix} 1 \\ 0 \end{bmatrix}. \tag{6-7}$$

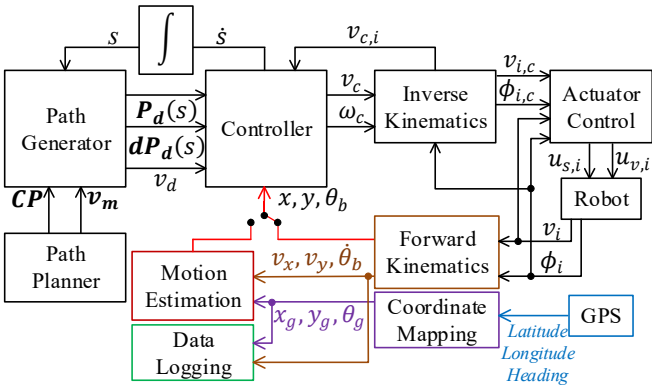

Fig. 4. Structure of the real-time control system with the new GPS (GNSS), Motion Estimation and Data Logging modules introduced in this study.

In (5), $\dot{\hat{Z}}_{\theta}$ and $\dot{\hat{b}}_{\theta}$ are the first derivatives of the fused heading angle and bias, and $k_{P,\theta}$ and $k_{I,\theta}$ are proportional and integral gains used for defining the dynamics of the filter. Term ω is a phenomenal part of the algorithm, and it is separately presented later in this section.

While using wheel odometry, the error in the heading angle, accumulated over time, will recursively affect to the accuracy of odometry-based x- and y-positions. For this reason, the fusion of the heading is conducted first and the fused signal $\hat{Z}_{\theta}$ is used in fusion of the positions. For fusion of the x- and y-positions, consider (8) and (9)

$$\begin{bmatrix} \dot{\hat{Z}}_{x} \\ \dot{\hat{b}}_{x} \end{bmatrix} = \boldsymbol{C}\begin{bmatrix} \hat{Z}_{x} \\ \hat{b}_{x} \end{bmatrix} + \omega_{x}\begin{bmatrix} k_{P,x} \\ k_{I,x} \end{bmatrix}(x_g - \hat{Z}_{x}) + \boldsymbol{D}\mathrm{v}_{\mathrm{bx}}^{\mathrm{w}}\cos\hat{Z}_{\theta}, \tag{8}$$

$$\begin{bmatrix} \dot{\hat{Z}}_{y} \\ \dot{\hat{b}}_{y} \end{bmatrix} = \boldsymbol{C}\begin{bmatrix} \hat{Z}_{y} \\ \hat{b}_{y} \end{bmatrix} + \omega_{y}\begin{bmatrix} k_{P,y} \\ k_{I,y} \end{bmatrix}(y_g - \hat{Z}_{y}) + \boldsymbol{D}\mathrm{v}_{\mathrm{bx}}^{\mathrm{w}}\sin\hat{Z}_{\theta}, \tag{9}$$

where $\mathrm{v}_{\mathrm{bx}}^{\mathrm{w}}$ is the incremental velocity measured along x-axis of the base frame {b}, and $\mathrm{x_g}$ and $\mathrm{y_g}$ represent the GPS positions, mapped to the base frame from the frame $\{\mathrm{g}_1\}$ of the left GPS-antenna.

Gain Adaptation

Term ω is used to adaptively manipulate the gains of k_P and k_I in real-time. For $i = \{\theta, x, y\}$, consider (10)

$$\omega_i = \exp\left(-\left(\frac{\|i_g - \hat{Z}_i\|}{c_i}\right)^2\right) \tag{10}$$

where, c_i is a positive real number that determines sensitiveness of the exponential weight to the difference between the expected value and the measured value. For instance, if the measured value for x approaches to a close neighborhood of $\hat{Z}_x$, the coefficient $k_{P,x}$ becomes fully effective. However, if the value goes farer, the coefficient asymptotically converges to zero. The value of c_i should be adjusted based on the scale of the acceptable errors and variance of the measurement noises. Larger constant values of c_i makes the system more conservative and smaller values can increase undesirable oscillations caused by the noise propagation. For a measurement instrument with systematic noise, the value of c_i is comparable to the standard deviation value in a Gaussian noise distribution.

IV. Results

The test cases 1 and 2 were performed in Finnish winter conditions. The ground was covered with snow and some ice, which caused wheel slipping. It is notable that all the four test case results are conducted with identical tuning of the M-estimator's gain parameters and coefficient, such that for $i = \{\theta, x, y\}$: $k_{P,i} = 1$, $k_{I,i} = 1$, and $c_i = 0.1$.

A. Cases 1 and 2: Synchronized Fusion

Results from the performance evaluation of the fusion on triangle path are presented in Fig. 5. The path was intentionally selected first to challenge our path-following controller by changing the driving direction during the experiment, but for the same reason it was a demanding case for the fusion. Odometry, absolute-GPS, and fusion-based positions and their corresponding heading angles are shown in plots (a), (c), (d) and (e). Plot (b) presents the section marked with the red circle in (a), where the test-case robot changes the driving direction from forward drive to reverse. Results prove the solution robust to this type of behavior. Bias values of all the three fused signals are shown in (f).

To highlight the performance of the fusion, a comparison between the first derivatives of the GPS- and fusion-based heading angles was conducted. The results are shown in Table II. Results show significant improvements, especially in the maximum value, which decreased 7-fold over the GPS.

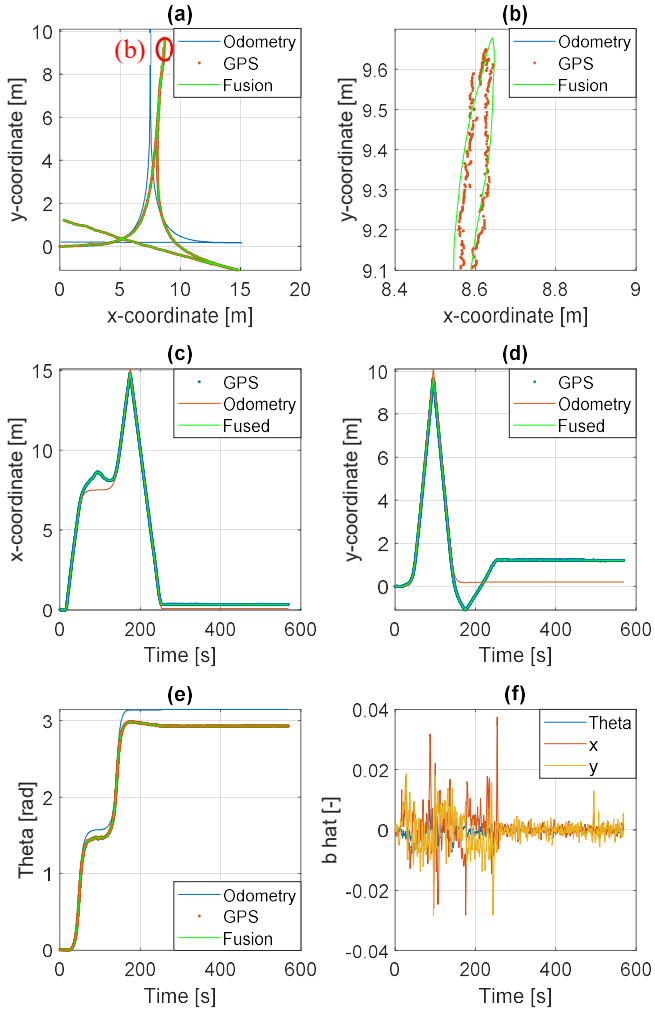

Fig. 5. Results from sensor fusion on triangular path (case 1).

TABLE II.
Rate of the heading angle based on GPS and fused signals (case 1).

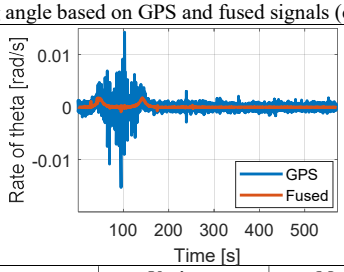

	Norm	*Variance*	*Maximum*
GPS	0.0978	3.2549	0.0143
Fusion	0.0549	0.9526	0.0018

Verifying the robustness to single point failures was conducted by manipulating the data by replacing some existing points with ones that clearly deviate from the expected path. In plots (a) and (b) it is shown that a single point deviation, 1.7 rad at the time point of 109.2 s, does not cause changes between the fused signals. As it is shown in (c) and (d), even a similar deviation that lasts for more than 1 s did not cause any unstable behavior, only a small deviation, which smoothly zeroed after receiving the GPS feedback again. This also proves the fusion robust to temporary GPS signal loss. With speeds less than 5 km/h, the path following can be continued multiple seconds before the recursive errors of the odometry start significantly increase the deviation from the true desired path.

Results from backpropagation of the linear wheel velocities of the case 1 are presented in Fig. 7. Results prove that while our odometry estimations are based on pure kinematic calculations, the variance between the measured feedback and back propagated velocity is small. The rear left wheel had some failures while measuring the velocity between time points of 28 and 45 s. As shown by the backpropagation, our Forward Kinematics can handle these failures and the estimation has even smaller deviations.

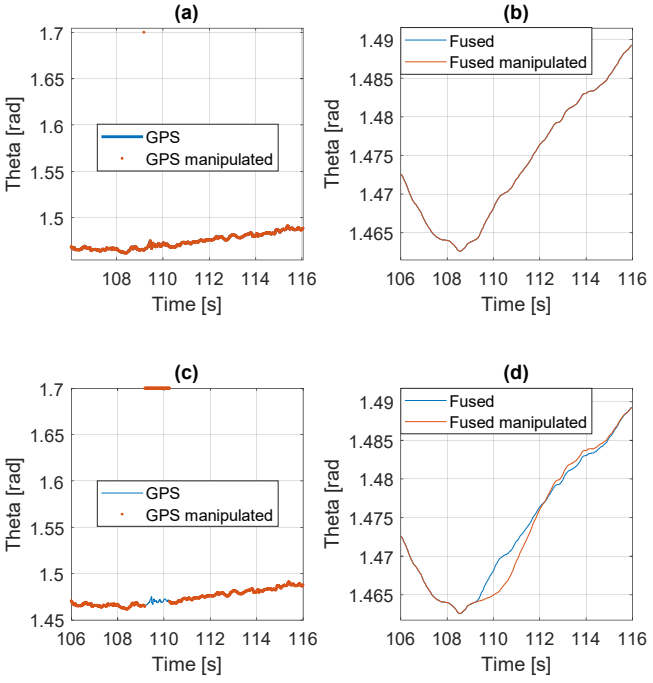

Fig. 6. Experimental results from proving the robustness of the fusion application to single point failures and temporary denial of GPS (case 1).

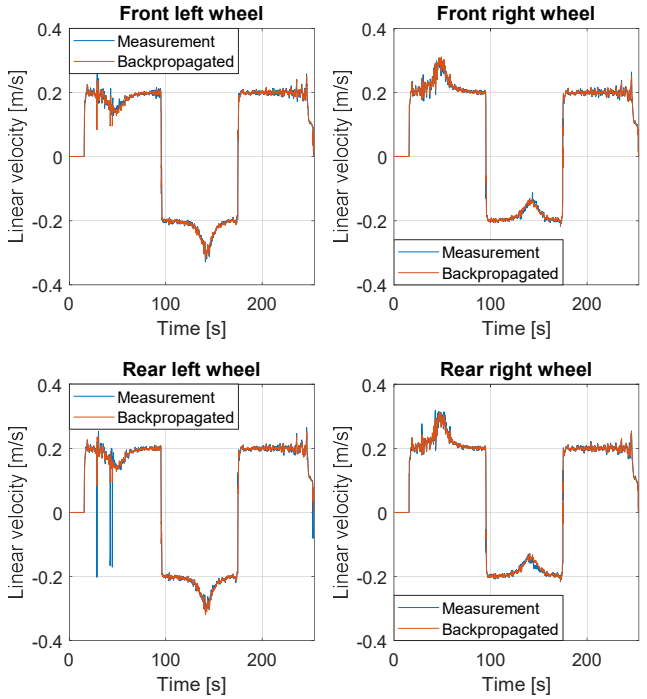

Fig. 7. Measured and back propagated wheel velocities of the case 1.

Experiments on different types of paths were conducted to highlight the feasibility of the fusion application under varying circumstances. Experimental results from a square type of path (case 2) are presented in Fig. 8. Plot (b) shows the smoothness of the fused signal while the GPS feedback had oscillations. While turning towards the same direction during the whole experiment, the recursive errors in the odometry signals (c-e) become visible.

B. Cases 3 and 4: Real-Time Fusion and Closed-Loop Control

Experimental results from closing the control loop with the real-time fusion feedback are illustrated in this section. In case 3, the plots (a-b) in Fig. 9 represent the same properties as the ones in Fig. 5 and Fig. 8. Heading fusion and bias values are shown in (c-d). The reference path and localization (Fusion) feedback of the path-following controller are shown in (e). Performance of the fusion and our controller by the means of position errors are shown in (f). The x- and y-errors describe the longitudinal and lateral errors between the reference path and control point of the robot, respectively. The mean error in the lateral path-following accuracy was 2.84 cm, while the maximum error was 9.75 cm.

Case 4 presents results from driving on a straight line using the closed-loop control with the fusion feedback. Plots (a-b) of Fig. 10 shows, how the fusion follows the absolute GPS-position accurately while it is smooth enough for the controller, so that both of the mean errors are less than 1 cm on a 9 m long path.

The results proved the fusion smooth and fast for the controller to drive the robot in a well-behaved manner. Due to time constraints, experiment cases 3 and 4 were the first one with the closed-loop fusion feedback, and, furthermore, none of the controller parameters were tuned yet for optimal control

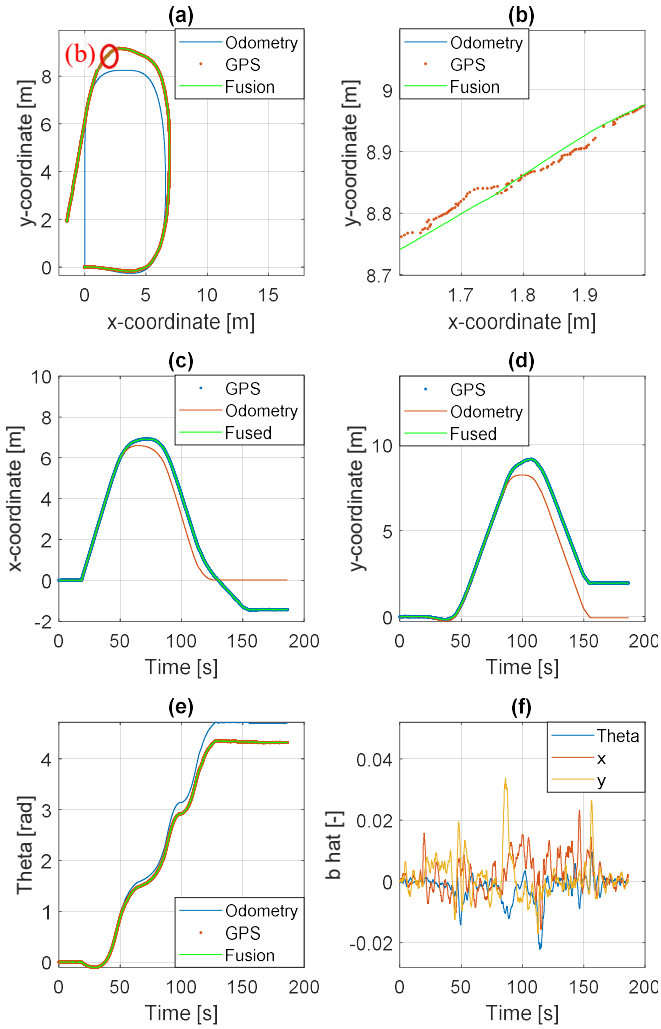

Fig. 8. Results from sensor fusion on square path (case 2).

performance. See the videos of our previous and future experiments conducted with the test-case robot[1].

Comparison between the key values of the first derivatives of GPS- and fusion-based heading angles are shown in Table III. The decreases in norm and variance were significant, even when comparing to the results of case 1 in Table II. Even the maximum value decreased 3-fold over the GPS on the harder test case 3. Due to the theoretical requirement of zero steering on a straight line, the fusion results of the case 4 were significantly better.

TABLE III.
Rate of the heading angle theta based on GPS and fused signals. Experiment cases 3 and 4.

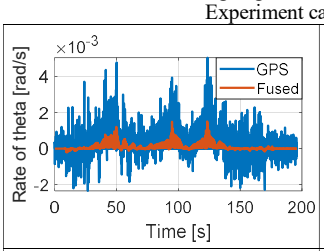

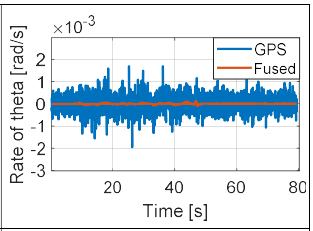

	Case 3			Case 4		
	Norm	*Var.*	*Max.*	*Norm*	*Var.*	*Max.*
GPS	0.0922	0.4880	0.0050	0.0210	0.0636	0.0017
Fusion	0.0222	0.0215	0.0015	0.0013	0.0002	0.0001

[1] *See the YouTube playlist:* https://goo.gl/Yj14zt

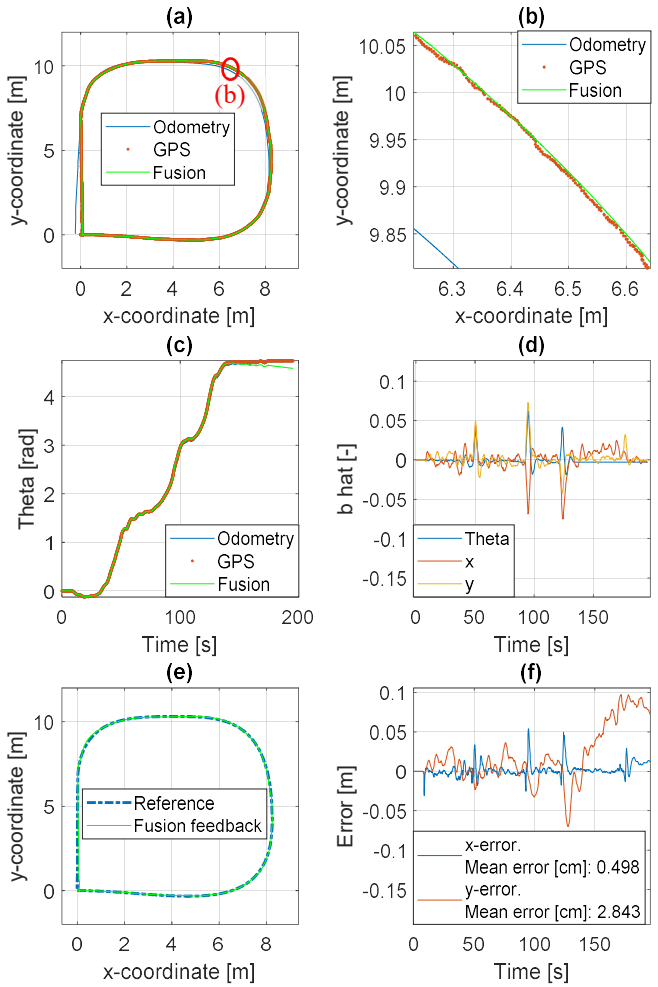

Fig. 9. Results from closing control loop with the fused feedback (Case 3).

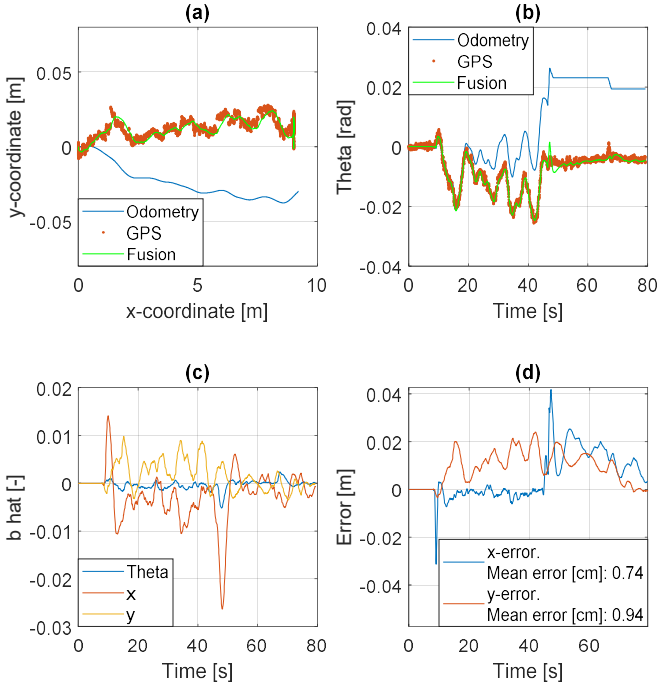

Fig. 10. Results from closing control loop with the fused feedback (Case 4).

V. Conclusion

The study presents a fusion between two types of position feedback signals: wheel odometry, which is smooth and has low latency, but is relative, and GPS that is absolute, but has jumps, noise and variable delay. The pure fusion results are shown in cases 1 and 2 of section IV, where the resulting signals are proven to be smooth, accurate and robust to temporary denial of the GPS, without introducing any delay. In cases 3 and 4, the application is used in real-time control system to provide a path-following controller with localization feedback. Results prove that the current setup provides suitable position feedback and the controller is able to drive the test-case robot on the predefined paths with longitudinal (x) and lateral (y) mean errors of 0.50 and 2.84 cm for case 3, and 0.74 and 0.94 cm for case 4. In these cases, the heading oscillations were reduced by 70 % and 95 %. These oscillations could cause unnecessary oscillations wasting energy in the steering actuators of the vehicle. Therefore, feedback smoothness plays a vital role in efficient and accurate control of the autonomous heavy-duty vehicle.

It is to be highlighted, that all parameters of the fusion application were the same in all of the four cases. This continues to validate the performance and robustness of our system in various scenarios. In the future research, the authors will continue improving the performance of the complete modular autonomous system, especially the fusion.

References

[1] Y.D. Setiawan, T.H. Nguyen, P.S. Pratama, H.K. Kim, and S.B. Kim, "Path tracking controller design of four-wheel independent steering automatic guided vehicle," International Journal of Control, Automation, and Systems, vol. 14, no. 6, 2016, pp. 1550–1560.

[2] R. Oftadeh, M. M. Aref, R. Ghabcheloo, and J. Mattila, "Bounded velocity motion control of four-wheel steered mobile robots," IEEE/ASME International Conference on Advanced Intelligent Mechatronics, Wollongong, Australia, 2013, pp. 255–260.

[3] R. Ghabcheloo, and S. Siddiqui, "Complete odometry estimation of a vehicle using single automotive Radar and a gyroscope," 26th Mediterranean Conference on Control and Automation (MED), Zadar, Croatia, 2018, pp. 855–860.

[4] P. Goel, S. I. Roumeliotis, and G. S. Sukhatme, "Robust localization using relative and absolute position estimates," IEEE/RSJ International Conference on Intelligent Robots and Systems. Human and Environment Friendly Robots with High Intelligence and Emotional Quotients, Kyongju, South Korea, 1999, pp. 1134–1140.

[5] H. Kim, C.W. Roh, S.C. Kang, and M.Y. Park, "Outdoo Navigation of a Mobile Robot Using Differential GPS and Curb Detection," IEEE/ICRA International Conference on Robotics and Automation, Roma, Italy, 2007, pp. 3414–3419.

[6] M. M. Aref, J. Vihonen, R. Ghabcheloo, and J. Mattila, " On Latencies and Noise Effects in Vision-Based Control of Mobile Robots," RAAD: Advances in Service and Industrial Robotics, Mechanisms and Machine Science, vol. 49, 2017, pp. 191–199.

[7] H. Liikanen, M. M. Aref, R. Oftadeh, and J. Mattila, "Path-Following Controller for 4WDs Hydraulic Heavy-Duty Field Robots with Nonlinear Internal Dynamics," 10th IFAC Symposium on Intelligent Autonomous vehicles (IAV), Gdansk, Poland, 2019, in press.

[8] M. M. Aref, R. Ghabcheloo, and J. Mattila, "A macro-micro controller for pallet picking by an articulated-frame-steering hydraulic mobile machine," IEEE/ICRA International Conference on Robotics and Automation, Hong Kong, China, 2014, pp. 6816–6822.

[9] R. Oftadeh, M. M. Aref, R. Ghabcheloo, and J. Mattila, "Mechatronic design of a four wheel steering mobile robot with fault-tolerant odometry feedback," 6th IFAC Symposium on Mechatronic Systems, Hangzhou, China, 2013, pp. 663–669.